chemosensors

MDPI

Article

Polyethyleneimine-MOF-235 Composite-Enhanced Electrochemical Detection of Silver Nanoparticles in Cosmetics

Shuo Duan [1,2,*] and Huang Dai [2]

[1] Department of Environment and Quality Test, Chongqing Chemical Industry Vocational College, Chongqing 401220, China
[2] College of Food Science and Engineering, Wuhan Polytechnic University, Wuhan 430023, China; huangdai9@126.com
* Correspondence: jcxy20241004@cqcivc.edu.cn

Abstract

Silver nanoparticles (AgNPs) are extensively utilized in cosmetics and healthcare products, creating an urgent need for sensitive quantification methods. We report the first application of a metal–organic framework for electrochemical AgNPs sensing in cosmetic samples. A glassy carbon electrode was modified with polyethyleneimine-encapsulated MOF-235 (PEI-MOF-235/GCE); the PEI layer enriches AgNPs through Ag–N coordination, whereas the high-surface-area MOF catalyzes their oxidative dissolution. Under optimized conditions (catalyst loading 1.4 μg mm^{-3}, pH 4.3 PBS), differential-pulse voltammetry provided a linear range of 10–100 ng L^{-1} and a detection limit of 3.93 ng L^{-1} (S/N = 3). The sensor exhibited excellent stability (RSD $\leq$ 4.7%) and good anti-interference capability toward common aquatic ions. Compared with a standard HPLC method, recoveries in spiked cosmetic samples were 97.9–102.6%. This MOF-based strategy offers a sensitive, selective, and field-deployable platform for routine monitoring of trace AgNPs.

Keywords: silver nanoparticles; polyethyleneimine; metal–organic frameworks; electrochemical sensing

check for updates

Received: 15 October 2025
Revised: 3 November 2025
Accepted: 4 November 2025
Published: 8 November 2025

Citation: Duan, S.; Dai, H. Polyethyleneimine-MOF-235 Composite-Enhanced Electrochemical Detection of Silver Nanoparticles in Cosmetics. *Chemosensors* **2025**, *13*, 392. https://doi.org/10.3390/chemosensors13110392

Copyright: © 2025 by the authors. Licensee MDPI, Basel, Switzerland. This article is an open access article distributed under the terms and conditions of the Creative Commons Attribution (CC BY) license (https://creativecommons.org/licenses/by/4.0/).

1. Introduction

Silver nanoparticles (AgNPs) have emerged as one of the most versatile nanomaterials in contemporary science and technology, finding extensive applications across diverse fields, including environmental treatment [1], medical antibacterial materials [2], photocatalysis [3], photoelectric conversion [4], cosmetics [5], and skincare products [6]. Their unique physicochemical properties, such as exceptional antimicrobial activity, surface plasmon resonance effects, and high electrical conductivity, have positioned them as indispensable components in numerous commercial and industrial applications [7]. However, the increasing prevalence of AgNPs in consumer products and industrial applications has raised significant concerns regarding their potential health hazards and environmental impacts [8]. Studies have demonstrated that AgNPs can induce cytotoxicity through multiple mechanisms, including oxidative stress, mitochondrial dysfunction, DNA damage, and inflammatory responses [9]. The small size and high surface reactivity of AgNPs enable them to penetrate biological barriers, potentially leading to systemic distribution and accumulation in vital organs such as the liver, spleen, kidneys, and brain. From an environmental perspective, the release of AgNPs into aquatic ecosystems can disrupt microbial communities, affect photosynthetic organisms, and bioaccumulate through the food chain, ultimately threatening ecosystem stability and biodiversity [10].

The cosmetic industry represents one of the most significant consumers of AgNPs, with their incorporation into various personal care products justified by their ability to prevent microbial growth, extend shelf life, and provide purported skin benefits [11]. The application value of AgNPs in cosmetics extends beyond simple preservation; they are marketed for their anti-inflammatory properties, wound healing capabilities, and potential anti-aging effects [12]. However, this widespread adoption has led to a concerning trend of AgNPs abuse, with some manufacturers incorporating excessive concentrations or utilizing inadequately characterized nanoparticles to enhance product appeal [13]. Silver nanoparticles (AgNPs) are increasingly incorporated into cosmetics as antimicrobial and preservative agents. However, the abuse of AgNPs is particularly problematic given the direct and prolonged skin contact associated with cosmetic products, which can facilitate nanoparticle penetration and systemic absorption. For example, AgNPs can penetrate the epidermis, accumulate in keratinocytes and fibroblasts, and trigger dose-dependent cytotoxicity evidenced by decreased viability, membrane leakage, and oxidative stress. Comet and chromosomal aberration assays reveal that even sub-cytothelial concentrations induce DNA breaks, micronuclei, and mutagenic lesions, indicating genotoxic potential. Repeated topical exposure facilitates trans-epidermal absorption, allowing AgNPs to reach systemic circulation and deposit in the liver, kidney, and spleen, where they generate reactive oxygen species, suppress antioxidant enzymes, elevate pro-inflammatory cytokines (TNF-α, IL-6), and provoke histopathological changes such as hepatocyte swelling and renal tubular necrosis. Furthermore, AgNPs may disrupt the cutaneous microbiome, compromise barrier integrity, and sensitize skin to secondary irritants. These cumulative data demonstrate that the cosmetic use of AgNPs presents risks of local irritation, genetic damage, organ toxicity, and chronic inflammation, necessitating rigorous safety evaluation, strict concentration limits, and surface modification strategies to minimize consumer exposure [14]. The potential health risks are further exacerbated by the lack of comprehensive regulations governing AgNPs concentrations in cosmetics and the absence of standardized safety assessment protocols.

The development of reliable and sensitive detection methods for AgNPs has therefore become a critical priority in ensuring consumer safety and environmental protection. Current analytical approaches for AgNPs detection encompass a range of techniques, including inductively coupled plasma mass spectrometry (ICP-MS) [15,16], UV–visible spectroscopy [17], and electrochemical methods. Mass spectrometry-based methods, including ICP-MS [15] and related single-particle ICP-MS [16], offer exceptional sensitivity and the ability to distinguish between ionic and nanoparticulate silver forms. However, they require extensive sample preparation, expensive instrumentation, and specialized operational expertise. UV–visible spectroscopy represents a simpler alternative, capitalizing on the characteristic surface plasmon resonance absorption of AgNPs, typically observed between 380 and 450 nm depending on particle size and surrounding medium. While this method provides rapid qualitative assessment, its quantitative capabilities are limited by matrix effects and the inability to distinguish between different silver species.

Electrochemical methods have gained considerable attention as promising alternatives for AgNPs detection, offering advantages including cost-effectiveness, portability, rapid analysis, and minimal sample preparation requirements [18–21]. Our group has developed relevant studies on the electrochemical detection of AgNPs, including the application of polyethyleneimine-carbon nanotube modified electrode [19] and MoS_2-graphene modified electrode [21] to improve electrochemical sensing performances for AgNPs. However, there are often difficulties in the actual detection of silver nanoparticles, especially those in cosmetic samples. Low target concentration and complex sample matrix interference both pose challenges to electrochemical detection. Therefore, exploring high-sensitivity electro-

chemical sensing materials that are more suitable for the detection of silver nanoparticles still holds positive significance.

2. Experimental Section

2.1. Instruments and Reagents

Terephthalic acid, $FeCl_3$ $6H_2O$, $AgNO_3$, and Arabic gum were all purchased from Sigma-Aldrich Company (Shanghai, China). $NaBH_4$ and $NaClO_4$ were purchased from Sichuan Kelon Reagent Company (Chengdu, China). Ammonia water; HNO_3; ethanol; KOH, KH_2PO_4, and Na_2HPO_4; $K_3[Fe(CN)_6]$, $K_4[Fe(CN)_6]$, and N, N-dimethylformamide (DMF) were all purchased from Chongqing Chemical Reagent Company (Chongqing, China). The deionized water used in the experiment is made in our laboratory. The reagents used in this article, unless otherwise specified, are all of analytical grade. KH_2PO_4 and Na_2HPO_4 were diluted to prepare phosphate-buffer solutions (PBS) with different pH values.

The synthesis process was accomplished by instruments such as the DZF6020 vacuum drying oven (Baojing Electronic Technology Co., Ltd., Zhengzhou, China), the TDZ4-WS benchtop low-speed centrifuge (Changsha Xiangyi Co., Ltd., Changsha, China), the KS-150D ultrasonic cleaning instrument (Haishu Technology Co., Ltd., Ningbo, China), and the Mars6 microwave digestion instrument (American CEM Company, Poston, AZ, USA). The electrochemical test was carried out by the CHI660E electrochemical workstation produced by Shanghai Chenhua Company in China. The characterization by scanning electron microscopy (SEM) was accomplished by the S-4800 field emission scanning electron microscope of Hitachi Corporation, Japan. The small-angle diffraction (XRD) characterization was accomplished by the XD-3 diffractometer of Beijing Puxi, China. The Fourier Transform Infrared spectroscopy (FT-IR) test was carried out by the 170SX spectrometer (Nicolet Company, Madison, WI, USA). Inductively coupled plasma mass spectrometry (ICP-MS) was carried out by the Agilent 7850, Agilent Technologies, Santa Clara, CA, USA.

2.2. Material Synthesis and Electrode Fabrication

As shown in Figure 1, in this work, PEI-MOF-235 was synthesized and used as the modification material for the glassy carbon electrode. The obtained PEI-MOF-235/GCE can be applied in the electrochemical detection of AgNPs due to its good adsorption capacity for AgNPs.

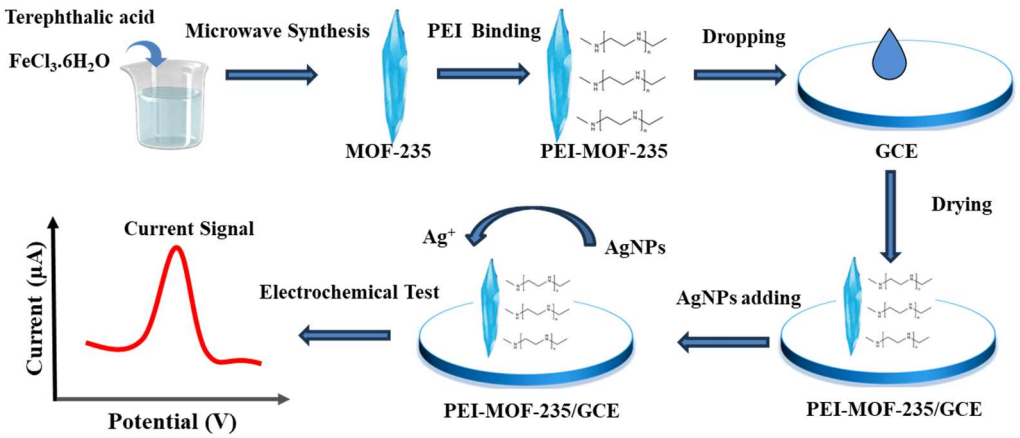


Figure 1. The scheme of the electrode preparation and the electrochemical sensing for AgNPs.

AgNPs standard solution: The synthetic method of AgNPs is referred to in the literature with slight modifications [22]. Briefly, 0.5 mL of 0.01 mol/L $AgNO_3$ solution was added drop by drop to 50 mL of 6 mg/mL Arabic gum solution, and stirred for 5 min. Then,

quickly add 2 mL of 2 mg/mL $NaBH_4$ solution and stir vigorously for 30 min to obtain AgNPs. The as-synthesized AgNPs colloid was subjected to centrifugation at 5000 rpm for 15 min; the supernatant was carefully discarded, and the pellet was re-dispersed in deionized water. This purification step was repeated twice. The final pellet was re-suspended in deionized water to yield a high-purity AgNPs solution. The obtained AgNPs solution was diluted with water to the appropriate concentration and then stored at a low temperature.

MOF-235: The synthesis of MOF-235 is based on previous studies [23,24]. Briefly, 0.205 g of terephthalic acid and 0.2 g of ferric chloride hexahydrate were dissolved in 60 mL DMF, and then 60 mL of ethanol was added and mixed in well. The mixed solution was transferred to the autoclave and heated in a closed environment at 80 °C for 24 h. After the reaction is completed, the mixed liquid is centrifuged at a rate of 3000 rpm, the lower solid layer is taken, and it is repeatedly washed with DMF and anhydrous ethanol. Finally, it is dried at 150 °C. The orange powder obtained is MOF-235.

PEI-MOF-235: The synthesis of PEI-MOF-235 was independently designed by our group. Briefly, 500 mg of PEI was ultrasonically dissolved in 500 mL of anhydrous ethanol to form a dispersion with a concentration of 1 mg/mL. Transfer 100 mL of the above dispersion, add 0.5 g of MOF-235 until dissolved, and stir magnetically at room temperature for 12 h to allow it to react. Add an appropriate amount of water until the pH of the solution is neutral. Subsequently, centrifuge at 3000 rpm, take the lower solid layer, and dry it at 45 °C. The orange powder obtained is PEI-MOF-235.

Electrode preparation: The glassy carbon electrode (GCCE) should be ultrasonically cleaned in ethanol until smooth before each use. PEI-MOF-235/GCE is prepared by drop coating a certain amount of PEI-MOF-235 dispersion on GCE. Similarly, PEI/GCE and MOF-235/GCE are prepared by drop coating PEI dispersion and MOF-235 dispersion, respectively.

2.3. Measurement and Sample Pretreatment

All the experiments in this chapter were conducted at room temperature. The electrochemical test adopts a three-electrode system, in which the silver/silver chloride (Ag/AgCl) electrode serves as the reference electrode, the platinum electrode as the auxiliary electrode, and GCE or modified GCE as the working electrode. Among them, cyclic voltammetry (CV), linear voltammetry (LSV), chronocoulometry (CC), differential pulse voltammetry (DPV), etc., were all conducted on the CHI660E electrochemical workstation. The electrolyte was selected as 0.1 M phosphate buffering solution (PBS) with pH = 4.3. The potential scanning ranges of CV and DPV were set from -0.4V to 0.6V. Meanwhile, the scanning range of CC was 0–0.4 V for $K_3[Fe(CN)_6]$ measurement and 0.1–0.6 V for AgNPs. The pulse amplitude and pulse width for DPV were 50 mV and 80 ms, respectively.

Pretreatment of cosmetic samples: The commercial hand cream was purchased from a local supermarket and studied as a cosmetic sample. Briefly, 1g of the cosmetic sample was first dissolved in 10 mL of isopropyl alcohol. After low-speed centrifugation for 30 min, the supernatant was removed. The bottom solid was transferred to 10mL of phosphate buffer solution, and a clear solution was formed under ultrasonic conditions. Repeat the above steps three times. The obtained clear solution is stored at a low temperature for future use.

3. Results and Discussion

3.1. Characterization of Electrode Materials

We prepared MOF-235 and PEI-MOF-235 as electrode materials for the subsequent electrochemical detection of AgNPs. To verify the reliability of the preparation method and the differences before and after PEI modification, we conducted a series of characterizations on the materials, including SEM, infrared spectroscopy, and XRD. The characterization

results are shown in Figure 2. The SEM characterization comparison images of MOF-235 before and after PEI modification are shown in Figure 2a,b. The microscopic morphology of MOF-235 in Figure 2a exhibits a distinct rod-conical structure with polyhedral morphology, which is basically consistent with the morphology reported in the literature [23,24]. After the PEI modification of MOF-235, the microstructure of PEI-MOF-235 obtained is shown in Figure 2b. PEI-MOF-235 still retains the rod-conical structure of MOF-235, meaning that the modification of PEI has not disrupted the original three-dimensional structure of MOF-235. Moreover, Figure 2b indicates that PEI has formed an irregular gel-like structure on the surface of MOF-235, indicating that PEI is well wrapped around the surface of MOF-235. The coating of PEI on the surface of MOF235 may provide excellent protection for MOF-235 and has a positive significance for enhancing the water stability of MOF-235.

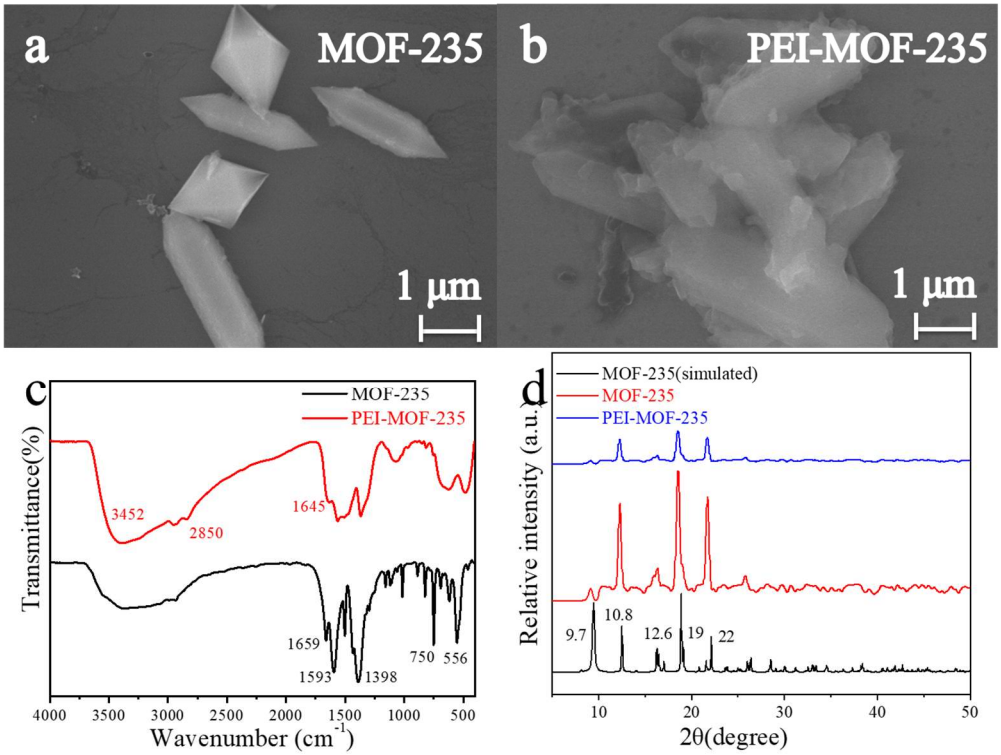


Figure 2. The SEM images for MOF-235 (**a**) and PEI-MOF-235 (**b**); the Raman spectra (**c**) and XRD patterns (**d**) for MOF-235 and PEI-MOF-235.

Infrared spectroscopy (IR) is an effective method for identifying compound types through specific chemical bonds. Figure 2c shows the IR spectra of MOF-235 and PEI- MOF-235. The synthesized MOF-235 exhibited distinct characteristic peaks at positions such as 556 cm^{-1}, 750 cm^{-1}, 1398 cm^{-1}, 1593 cm^{-1}, 1659 cm^{-1}, and 2890 cm^{-1}. This proves the successful synthesis of MOF-235 [23,24]. After PEI modification, PEI-MOF-235 retains most of the characteristic peaks of MOF-235, and the slight shift in the peak position is attributed to the encapsulation of the MOF structure by PEI. Meanwhile, characteristic peaks of PEI appeared at 1645 cm^{-1}, 2850 cm^{-1}, and 3452 cm^{-1} (corresponding, respectively, to the C-H bond and N-H bond in the PEI molecule), indicating that PEI was successfully applied on the surface of MOF-235 [25]. The XRD patterns of MOF-235 and PEI-MOF-235 prepared in this work are shown in Figure 2d. The XRD results of the MOF-235 prepared by us are highly consistent with the standard simulated pattern of MOF-235, which is in line with the literature reports. The five characteristic peaks, which are located at 9.7°, 10.8°, 12.6°, 19°, and 22°, were all reflected in the prepared MOF-235, indicating that the standard MOF-235 crystal was successfully prepared in this paper [23,24]. After PEI modification,

PEI-MOF-235 still possesses its five characteristic peaks, and the peak positions remain unchanged. This indicates that the modification of PEI did not change the crystal structure of MOF-235 itself.

3.2. Electrochemical Investigation and Characterization

To systematically evaluate the electrochemical behavior of the PEI-MOF-235 hybrid, the PEI-MOF-235/GCE was interrogated using $[Fe(CN)_6]^{3-/4-}$ as a benchmark redox probe and compared with bare GCE, PEI/GCE, and CNTs/GCE under identical conditions (Figure 3a). At the unmodified GCE, a quasi-reversible couple was observed with anodic and cathodic peaks centered at ca. +0.25 V and +0.20 V (vs. Ag/AgCl), respectively, corresponding to the $[Fe(CN)_6]^{3-/4-}$ redox transformation. Coating the surface with PEI alone did not alter peak potentials but produced a pronounced increase in peak currents, indicative of an electrostatic enrichment effect that accelerates interfacial electron transfer. Introduction of MOF-235 further amplified the faradaic response; however, two additional anodic features emerged at +0.20 V and +0.52 V, ascribed to the partial oxidation of Fe(III) nodes within the MOF lattice. These parasitic processes reflect the limited hydrolytic stability of the bare framework and may compromise the long-term reproducibility of MOF-235/GCE [26]. In contrast, the PEI-MOF-235/GCE exhibited the highest $[Fe(CN)_6]^{3-/4-}$ peak currents while completely suppressing the framework-associated oxidations. This observation demonstrates that the conformal PEI overlayer not only promotes charge transfer but also shields the MOF from aqueous degradation, thereby simultaneously enhancing sensitivity and operational stability.

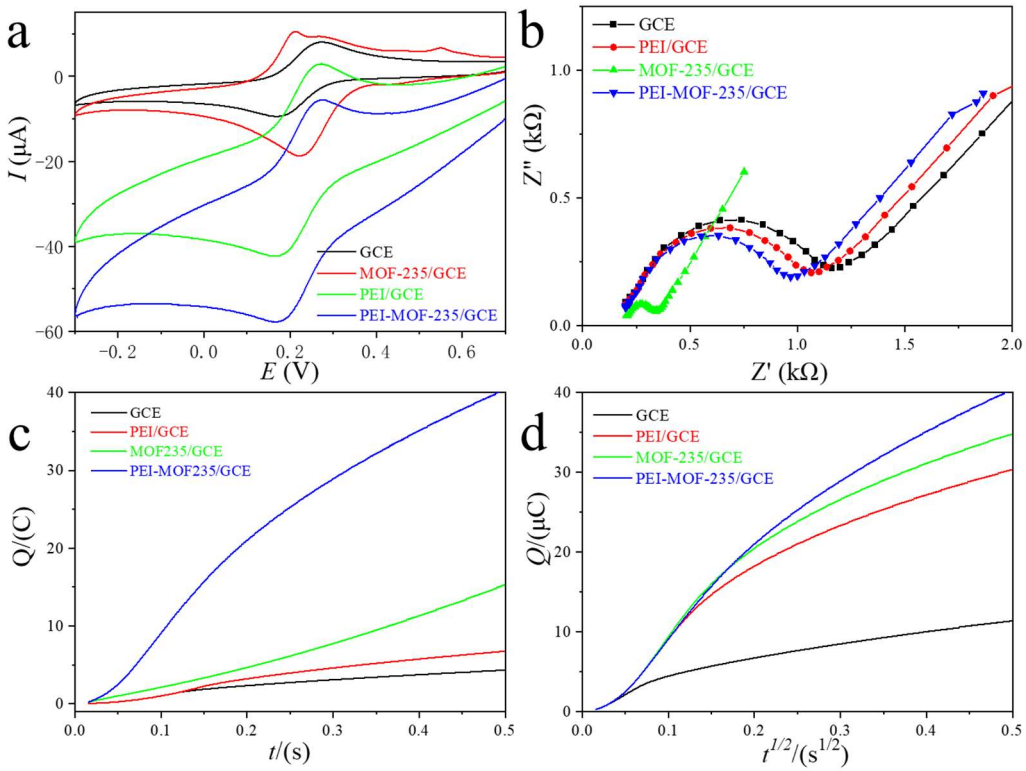


Figure 3. The CVs (**a**), EIS (**b**), and CCs (**c**,**d**) curves for bare GCE, PEI/GCE, MOF-235/GCE, and PEI-MOF-235/GCE in the electrolyte with 5mM of $[Fe(CN)_6]^{3-/4-}$ solution.

In electrochemical impedance spectroscopy (EIS), the Nyquist profile typically comprises a semicircle at high frequencies followed by a linear diffusion tail. The diameter of the semicircle is directly proportional to the interfacial charge-transfer resistance (R_{ct}); a larger arc signifies a higher kinetic barrier for electron transfer. As shown in Figure 2b, the

MOF-235/GCE exhibited a pronounced reduction in semicircle diameter than bare GCE, corroborating that the abundant, redox-accessible Fe(III) nodes within the MOF framework facilitate rapid interfacial electron exchange. Conversely, the PEI-MOF-235/GCE displayed a modest increase in arc diameter, indicating that the insulating, polycationic PEI sheath introduces an additional energetic penalty for charge transfer, thereby impeding conductivity despite its beneficial role in analyte enrichment and framework stabilization.

To further benchmark the interfacial properties of the four electrodes, chronocoulometry (CC) was performed. The Q-t and Q–$t^{1}/^{2}$ plots for bare GCE, PEI/GCE, MOF-235/GCE, and PEI-MOF-235/GCE in $[Fe(CN)_6]^{3-}/^{4-}$ solution were shown in Figures 3c and 3d, respectively. The Q-t plots indicated that PEI-MOF-235/GCE performed the highest slope in CC measurement, which was attributed to the large specific surface area of MOF materials and the abundant amino adsorption sites of PEI. According to the integrated Anson equation [26], the slope of the Q-$t^{1}/^{2}$ straight line is directly proportional to the electrochemically active surface area (ECSA). All four electrodes in Figure 3d exhibited excellent linearity, confirming diffusion-controlled kinetics. Strikingly, the slopes obtained for MOF-235/GCE and PEI-MOF-235/GCE were markedly steeper than those of GCE and PEI/GCE, reflecting both substantial porosity and the metal catalytic sites of the MOF framework. Quantitative analysis yielded EASA values of 0.0375 cm^2 for GCE, 0.121 cm^2 for PEI/GCE, 0.213 cm^2 for PEI-MOF-235/GCE, and 0.203 cm^2 for MOF-235/GCE. The pronounced enlargement observed for the MOF-modified electrodes underscores the pivotal role of the high-specific-area MOF-235 in furnishing abundant accessible sites for heterogeneous electron transfer.

To assess the practical applicability of the fabricated electrodes for silver nanoparticle (AgNP) quantification, their voltammetric responses were recorded in AgNP-spiked electrolytes. Figure 4a compares the cyclic voltammograms obtained at bare GCE, PEI/GCE, MOF-235/GCE, and PEI-MOF-235/GCE. At the unmodified GCE, a weak anodic peak was observed at 0.33 V (vs. Ag/AgCl), corresponding to the oxidative dissolution of AgNPs. Upon modification with PEI, the peak potential remained unchanged, but the peak current increased significantly, demonstrating that the amine-rich PEI layer effectively enriches AgNPs through electrostatic and coordinative interactions, thereby enhancing the faradaic response [27]. Introduction of MOF-235 further improved the performance: the oxidation potential shifted negatively to 0.31 V, and the peak current increased substantially. This indicates that (i) the porous MOF structure enhances local AgNP concentration via physical confinement and (ii) the Fe(III) nodes within the MOF framework exhibit electrocatalytic activity, lowering the activation energy for the $Ag^0 \rightarrow Ag^+$ conversion. Benefiting from the synergistic effects of AgNP enrichment by PEI and electrocatalysis by MOF-235, the PEI-MOF-235/GCE electrode demonstrated the highest performance, with a well-defined oxidation peak at 0.31 V and a peak current of 8.95 μA, significantly superior to those observed with the other three electrodes.

Chronocoulometry was subsequently employed to quantify the interfacial AgNPs coverage (Figure 4b). After subtraction of the background charge, the adsorption capacities (Q_{ads}) were determined to be 1.30×10^{-6} C (GCE), 2.59×10^{-6} C (PEI/GCE), 1.59×10^{-6} C (MOF-235/GCE), and 2.95×10^{-6} C (PEI-MOF-235/GCE). Normalization to the respective electrochemically active surface areas (Eq. 2.3, Q_{ads} = nF$A\Gamma$) yielded surface-excess values (Γ) of 7.7×10^{-11} mol cm^{-2} (MOF-235/GCE), 1.5×10^{-10} mol cm^{-2} (PEI-MOF-235/GCE), and 2.2×10^{-10} mol cm^{-2} (PEI/GCE). The superior Γ obtained for PEI-containing interfaces confirms that the amine-rich polymer dominates the interfacial capture of AgNPs, while the MOF component primarily provides catalytic and surface-area enhancements.

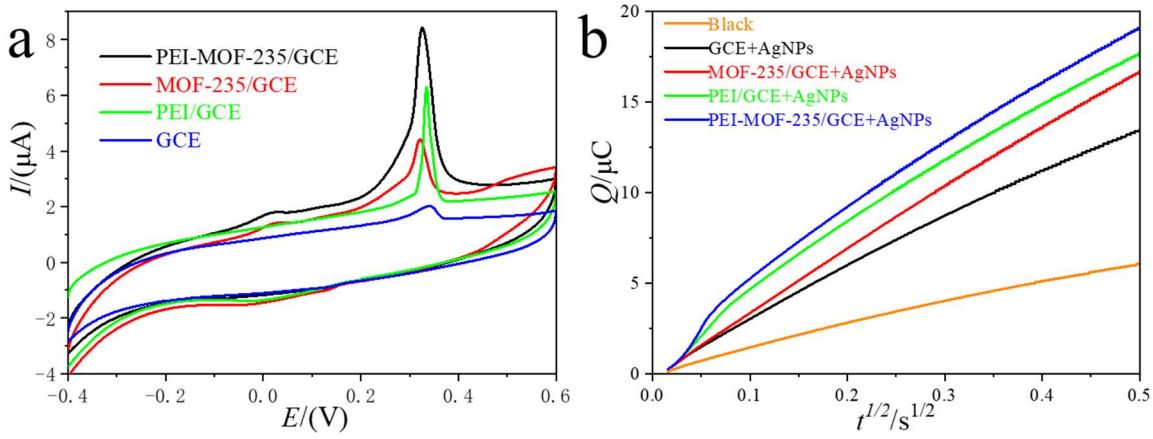


Figure 4. The CVs (**a**) and CC (**b**) curves of AgNPs for bare GCE, PEI/GCE, MOF-235/GCE, and PEI-MOF-235/GCE in the electrolyte with 20 ng/L of AgNPs.

The above findings demonstrate that the PEI-MOF-235/GCE synergistically combines the high Ag^0-affinity of polyethyleneimine with the large specific surface area of MOF-235, thereby significantly promoting the electrochemical oxidation of silver nanoparticles. This dual effect endows the modified electrode with excellent sensitivity and establishes a promising platform for the electroanalytical determination of AgNPs.

3.3. Electrochemical Detection of AgNPs at PEI-MOF-235/GCE

The influence of catalyst loading and electrolyte pH on the voltammetric response toward AgNPs at PEI-MOF-235/GCE was systematically investigated. As shown in Figure 5a, when the PEI-MOF-235 loading was increased from 0.2 to 1.4 μg mm^{-3}, the anodic peak current of AgNPs rose monotonically, reflecting the higher density of accessible active sites. Conversely, loadings exceeding 1.4 μg mm^{-3} produced a progressive current decline, attributed to the formation of an overly thick film that impedes electron transfer. Consequently, an optimal loading of 1.4 μg mm^{-3} was adopted for all subsequent measurements.

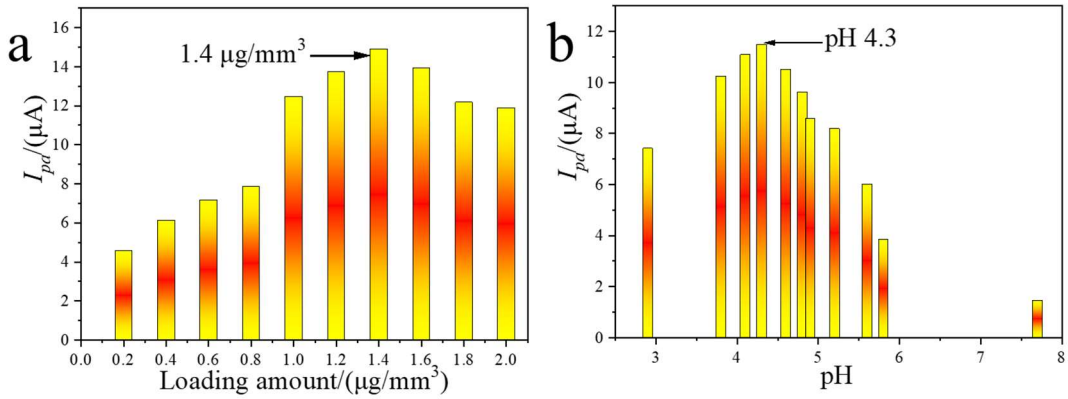


Figure 5. Optimization of the loading amount of catalysts (**a**) and pH value (**b**) for AgNPs determination.

Electrolyte pH is another critical parameter governing the interfacial chemistry. A series of PBS buffers covering the range 2.8–7.7 was prepared by varying the NaH_2PO_4/Na_2HPO_4 ratio, and the resulting peak currents are plotted in Figure 5b. Between pH 4.3 and 7.7, the current decreased steadily with increasing pH; this trend is rationalized by the diminishing surface positive charge of PEI-MOF-235 as the concentration of H^+ declines, weakening electrostatic attraction toward negatively charged AgNPs. Below pH 4.3, the current again diminished, most likely because excessive protonation

of the PEI amines disrupts their coordination affinity for Ag^0. The maximum response was therefore obtained at pH 4.3, which was selected as the optimum electrolyte pH for analytical work.

Differential pulse voltammetry (DPV) superimposes a short voltage pulse on a linear ramp, markedly suppressing non-faradaic (charging) currents and consequently enhancing analytical sensitivity. Exploiting this advantage, we developed a DPV-based protocol for AgNPs under the previously optimized conditions: catalyst loading 1.4 μg mm^{-3} and pH 4.3 PBS. Figure 6a displays the DPV curves recorded for AgNPs concentrations spanning 10–100 ng L^{-1}. The oxidative dissolution peak remained fixed at +0.27 V (vs. Ag/AgCl), while its magnitude increased monotonically with AgNPs concentration. The calibration plot, shown in Figure 6b, displayed the linear relationship with peak current (I_{pa}) versus concentration (c) is linear over the entire range, obeying the equation: I_{pa} (μA) = 2.164 + 0.2207 c (ng L^{-1}), with a correlation coefficient R^2 = 0.9870. From the slope and three times the standard deviation of the blank (3σ), a limit of detection (LOD) of 3.93 ng L^{-1} was calculated. Compared with previously reported AgNP-based electrochemical sensors (Table 1), the PEI-MOF-235/GCE exhibits a more favorable operating potential and a lower limit of detection than most, highlighting its competitive advantage for sensitive quantification.

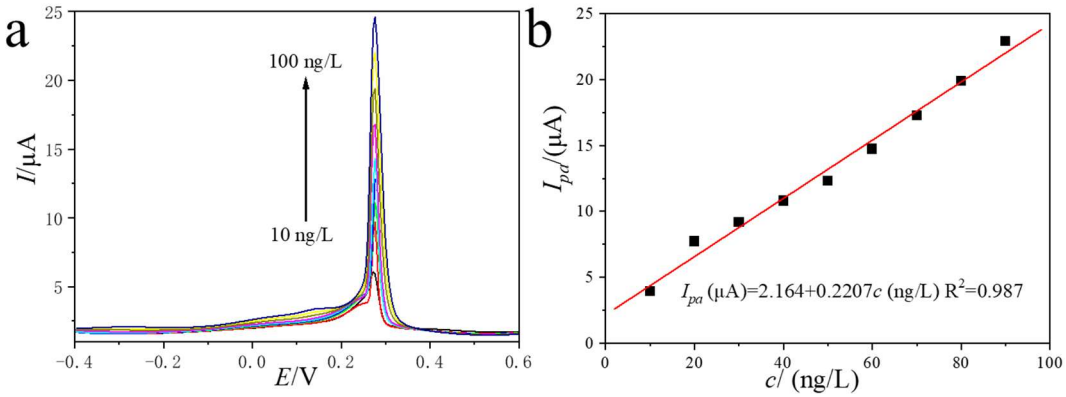


Figure 6. The DPV results for AgNPs with a concentration range from 10 to 100 ng/L at PEI-MOF-235/GCE (**a**); the corresponding linear relationship between the peak currents and the concentration of AgNPs (**b**).

Table 1. Analytical performance comparison for electrochemical methods for AgNP detection.

Working Electrode	Peak Potential (Normalized vs. Ag/AgCl, V)	LOD (Normalized, g/L)	Linear Relationship (Normalized, ng/L)	Reference
Macro-GCE	0.42	N/A	N/A	[19]
SPE	0.31	5×10^{-7}	N/A	[28]
GCE	0.24	3.31×10^{-8}	33.1–500	[29]
Pt disk electrode	0.61	N/A	N/A	[30]
Poly(amic) acid filter membrane electrode	0.23	1.4×10^{-4}	N/A	[31]
GC microelectrode	0.27	1×10^{-4}	500–20,000	[32]
DMSA/gold electrode	0.37–0.51	N/A	N/A	[33]
Carbon fiber microelectrode	0.19	N/A	N/A	[34]
MoS_2-rGO/GCE	0.27	2.63×10^{-9}	5–120	[21]
PEI-MOF-235/GCE	0.26	3.93×10^{-9}	10–100	This work

Stability, reproducibility, and selectivity are critical figures of merit for any electroanalytical protocol. Under the optimized conditions, repetitive DPV measurements (n = 6) of a 50 ng L^{-1} AgNPs standard yielded a relative standard deviation (RSD) of 2.7%, while six independently fabricated PEI-MOF-235/GCE sensors gave an RSD of 4.7% for the same sample. These low RSD values attest to excellent intra-day precision and inter-electrode reproducibility. Interference studies were conducted by spiking a 100 ng L^{-1}

AgNPs solution with common aqueous matrix ions: 0.1 mol L^{-1} Na^+, K^+, and PO_4^{3-}; 1 mmol L^{-1} Ca^{2+}, Mg^{2+}, and NH_4^+; 0.1 mmol L^{-1} SO_4^{2-} and NO_3^-; and 100 μg L^{-1} Cu^{2+}, Pb^{2+}, and Cd^{2+}. None of these species altered the AgNPs peak current by more than ±5%, although their concentrations far exceeded both the target level and the limits stipulated by the European Union water-quality directives. The proposed method, therefore, exhibits satisfactory selectivity for real-sample analysis. Simulated cosmetic samples (pH adjusted to 4.3) were analyzed after 3 h pre-concentration in 10 mL PBS containing 5 mmol L^{-1} $NaClO_4$ to mask chloride. Each sample was tested five times, and the corresponding average value and recovery rate were calculated. Standard-addition DPV gave recoveries of 97.9–102.6% (Table 2), confirming the reliability of the PEI-MOF-235/GCE sensor for trace AgNPs determination in cosmetic samples. Further verification was conducted using the inductively coupled plasma mass spectrometry (ICP-MS) method. The data obtained by this method show a high degree of consistency with that obtained by ICP-MS, and its recovery rate is 95.9–98.1%.

Table 2. Standard addition measurement for AgNPs detection in cosmetic sample (n = 5).

Adding Mount (ng/L)	Electrochemical Detected Amount (ng/L)	Electrochemical Recovery (%)	ICP-MS Validation Recovery (%)
0	-	-	
10.0	9.83 ± 0.2	98.3	97.6
30.0	28.2 ± 0.3	94.0	95.9
50.0	49.7 ± 0.3	99.4	98.1

4. Conclusions

In this work, MOF-235 was successfully synthesized and subsequently encapsulated with polyethyleneimine (PEI) to afford the PEI-MOF-235 composite. Compared to the parent MOF-235, the hybrid material exhibited markedly enhanced electrochemical stability. When deployed as a surface modifier on a glassy carbon electrode (GCE), the PEI-MOF-235 film synergistically combined the Ag-affinity of the amine-rich PEI layer with the high specific surface area of the MOF scaffold, resulting in a significant amplification of the oxidative signal for silver nanoparticles (AgNPs). Additionally, PEI encapsulation effectively shielded the MOF lattice from hydrolytic degradation, further improving operational durability.

Under optimized conditions, the PEI-MOF-235/GCE sensor delivered a limit of detection of 3.93 ng L^{-1} for AgNPs, together with excellent stability (RSD ≤ 4.7%) and selectivity in the presence of common environmental interferents. To the best of our knowledge, this constitutes the first report of a MOF-based electrochemical platform dedicated to AgNPs quantification. The strategy not only expands the analytical utility of MOFs but also offers a sensitive, reliable, and field-deployable method for trace AgNPs monitoring in complex cosmetic matrices.

Author Contributions: Conceptualization, S.D. and H.D.; methodology, H.D.; software, H.D.; validation, S.D.; formal analysis, S.D.; investigation, S.D.; resources, H.D.; data curation, H.D.; writing—original draft preparation, S.D.; writing—review and editing, S.D.; visualization, S.D.; supervision, S.D.; project administration, S.D.; funding acquisition, S.D. All authors have read and agreed to the published version of the manuscript.

Funding: This research was funded by the Chongqing Natural Science Foundation (No. 2024NSCQ-MSX0774) and the Scientific research project of Chongqing Education Committee (No. KJQN202404503).

Institutional Review Board Statement: Not applicable.

Informed Consent Statement: Not applicable.

Data Availability Statement: The original contributions presented in this study are included in the article. Further inquiries can be directed to the corresponding author.

Acknowledgments: Acknowledgments for Yuming Huang. The authors have reviewed and edited the output and take full responsibility for the content of this publication.

Conflicts of Interest: The authors declare no conflicts of interest.

References

1. Rafeeq, H.; Hussain, A.; Ambreen, A.; Zill-e-Huma; Waqas, M.; Bilal, M.; Iqbal, H.M.N. Functionalized nanoparticles and their environmental remediation potential: A review. *J. Nanostruct. Chem.* **2022**, *12*, 1007–1031. [CrossRef]
2. Naganthran, A.; Verasoundarapandian, G.; Khalid, F.E.; Masarudin, M.J.; Zulkharnain, A.; Nawawi, N.M.; Karim, M.; Abdullah, C.M.C.; Ahmad, S.A. Synthesis, characterization and biomedical application of silver nanoparticles. *Materials* **2022**, *15*, 427. [CrossRef]
3. Rani, P.; Kumar, V.; Singh, P.P.; Matharu, A.S.; Zhang, W.; Kim, K.-H.; Singh, J.; Rawat, M. Highly stable AgNPs prepared via a novel green approach for catalytic and photocatalytic removal of biological and non-biological pollutants. *Environ. Int.* **2020**, *143*, 105924. [CrossRef]
4. Sharma, R.K.; Yadav, S.; Dutta, S.; Kale, H.B.; Warkad, I.R.; Zbořil, R.; Varma, R.S.; Gawande, M.B. Silver nanomaterials: Synthesis and (electro/photo) catalytic applications. *Chem. Soc. Rev.* **2021**, *50*, 11293–11380. [CrossRef]
5. Arroyo, G.V.; Madrid, A.T.; Gavilanes, A.F.; Naranjo, B.; Debut, A.; Arias, M.T.; Angulo, Y. Green synthesis of silver nanoparticles for application in cosmetics. *J. Environ. Sci. Health Part A* **2020**, *55*, 1304–1320. [CrossRef] [PubMed]
6. Szczepańska, E.; Bielicka-Giełdoń, A.; Niska, K.; Strankowska, J.; Żebrowska, J.; Inkielewicz-Stępniak, I.; Łubkowska, B.; Swebocki, T.; Skowron, P.; Grobelna, B. Synthesis of silver nanoparticles in context of their cytotoxicity, antibacterial activities, skin penetration and application in skincare products. *Supramol. Chem.* **2020**, *32*, 207–221. [CrossRef]
7. Beyene, H.D.; Werkneh, A.A.; Bezabh, H.K.; Ambaye, T.G. Synthesis paradigm and applications of silver nanoparticles (AgNPs), a review. *Sustain. Mater. Technol.* **2017**, *13*, 18–23. [CrossRef]
8. Massarsky, A.; Trudeau, V.L.; Moon, T.W. Predicting the environmental impact of nanosilver. *Environ. Toxicol. Pharmacol.* **2014**, *38*, 861–873. [CrossRef]
9. Sondi, I.; Salopek-Sondi, B. Silver nanoparticles as antimicrobial agent: A case study on E. coli as a model for Gram-negative bacteria. *J. Colloid Interface Sci.* **2004**, *275*, 177–182. [CrossRef]
10. Sun, X.; Shi, J.; Zou, X.; Wang, C.C.; Yang, Y.; Zhang, H.W. Silver nanoparticles interact with the cell membrane and increase endothelial permeability by promoting VE-cadherin internalization. *J. Hazard. Mater.* **2016**, *317*, 570–578. [CrossRef]
11. Patel, A.; Prajapati, P.; Boghra, R. Overview on application of nanoparticles in cosmetics. *Asian J. Pharm. Clin. Res.* **2011**, *1*, 40–55.
12. Xi, J.; Kan, W.; Zhu, Y.; Huang, S.W.; Wu, L.F.; Wang, J. Synthesis of silver nanoparticles using Eucommia ulmoides extract and their potential biological function in cosmetics. *Heliyon* **2022**, *8*, 8. [CrossRef] [PubMed]
13. Salvioni, L.; Galbiati, E.; Collico, V.; Alessio, G.; Avvakumova, S.; Corsi, F.; Tortora, P.; Prosperi, D.; Colombo, M. Negatively charged silver nanoparticles with potent antibacterial activity and reduced toxicity for pharmaceutical preparations. *Int. J. Nanomed.* **2017**, *12*, 2517–2530. [CrossRef]
14. Gupta, R.; Xie, H. Nanoparticles in daily life: Applications, toxicity and regulations. *J. Environ. Pathol. Toxicol. Oncol.* **2018**, *37*, 209–230. [CrossRef]
15. Mitrano, D.M.; Barber, A.; Bednar, A.; Westerhoff, P.; Higginsd, C.P.; Ranville, J.F. Silver nanoparticle characterization using single particle ICP-MS (SP-ICP-MS) and asymmetrical flow field flow fractionation ICP-MS (AF4-ICP-MS). *J. Anal. At. Spectrom.* **2012**, *27*, 1131–1142. [CrossRef]
16. Roman, M.; Rigo, C.; Castillo-Michel, H.; Munivrana, I.; Vindigni, V.; Mičetić, I.; Benetti, F.; Manodori, L.; Cairns, W.R.L. Hydrodynamic chromatography coupled to single-particle ICP-MS for the simultaneous characterization of AgNPs and determination of dissolved Ag in plasma and blood of burn patients. *Anal. Bioanal. Chem.* **2016**, *408*, 5109–5124. [CrossRef] [PubMed]
17. Lodeiro, P.; Achterberg, E.P.; Pampín, J.; Affatati, A.; El-Shahawi, M.S. Silver nanoparticles coated with natural polysaccharides as models to study AgNP aggregation kinetics using UV-Visible spectrophotometry upon discharge in complex environments. *Sci. Total Environ.* **2016**, *539*, 7–16. [CrossRef]
18. Zhou, Y.; Rees, N.V.; Compton, R. The electrochemical detection and characterization of silver nanoparticles in aqueous solution. *Angew. Chem. Int. Ed.* **2011**, *50*, 18. [CrossRef]
19. Stuart, E.J.E.; Tschulik, K.; Omanović, D.; Cullen, J.T.; Jurkschat, K.; Crossley, A.; Compton, R.G. Electrochemical detection of commercial silver nanoparticles: Identification, sizing and detection in environmental media. *Nanotechnology* **2013**, *24*, 444002. [CrossRef]

20. Duan, S.; Yue, R.; Huang, Y. Polyethylenimine-carbon nanotubes composite as an electrochemical sensing platform for silver nanoparticles. *Talanta* **2016**, *160*, 607–613. [CrossRef]
21. He, J.I.; Duan, S.; Yue, R.; Zhang, X.; Wang, Q.; Xu, L.; Liu, Y.; Fang, M.; Yang, Q. High sensitive electrochemical detection of silver nanoparticles based on a MoS2/graphene composite. *J. Nanopart. Res.* **2022**, *24*, 92. [CrossRef]
22. Al-Ansari, M.M.; Al-Dahmash, N.D.; Ranjitsingh, A.J.A. Synthesis of silver nanoparticles using gum Arabic: Evaluation of its inhibitory action on Streptococcus mutans causing dental caries and endocarditis. *J. Infect. Public Health.* **2021**, *14*, 324–330. [CrossRef] [PubMed]
23. Anbia, M.; Hoseini, V.; Sheykhi, S. Sorption of methane, hydrogen and carbon dioxide on metal-organic framework, iron terephthalate (MOF-235). *J. Ind. Eng. Chem.* **2012**, *18*, 1149–1152. [CrossRef]
24. Haque, E.; Jun, J.W.; Jhung, S.H. Adsorptive removal of methyl orange and methylene blue from aqueous solution with a metal-organic framework material, iron terephthalate (MOF-235). *J. Hazard. Mater.* **2011**, *185*, 507–511. [CrossRef]
25. Gilmer, D.B.; Han, L.; Lehmann, M.L.; Siddel, D.H.; Yang, G.; Chowdhury, A.U.; Doughty, B.; Elliott, A.M.; Saito, T. Additive manufacturing of strong silica sand structures enabled by polyethyleneimine binder. *Nat. Commun.* **2021**, *12*, 5144. [CrossRef]
26. Brown, A.P.; Anson, F.C. Cyclic and differential pulse voltammetric behavior of reactants confined to the electrode surface. *Anal. Chem.* **1977**, *49*, 1589–1595. [CrossRef]
27. Batista, L.C.D.; Santos, T.I.S.; Santos, J.E.L.; da Silva, D.R.; Martínez-Huitle, C.A. Metal organic framework-235 (MOF-235) modified carbon paste electrode for catechol determination in water. *Electroanalysis* **2021**, *33*, 57–65. [CrossRef]
28. Cepriá, G.; Córdova, W.R.; JiménezLamana, J.; Laborda, F.; Castillo, J.R. Silver nanoparticle detection and characterization in silver colloidal products using screen printed electrodes. *Anal. Methods* **2014**, *6*, 3072. [CrossRef]
29. Goda, T.; Ambrosi, A.; Miyahara, Y.; Pumera, M. Simultaneous Electrochemical Detection of Silver and Molybdenum Nanoparticles. *ChemElectroChem* **2014**, *1*, 529–531. [CrossRef]
30. Chaudhari, V.R.; Hassan, P.A.; Haram, S.K. Size-dependent quantized double layer charging of monolayer-protected silver nanoparticles. *New J. Chem.* **2014**, *38*, 1761–1767. [CrossRef]
31. Li, X.; Batchelor-McAuley, C.; Compton, R.G. Silver nanoparticle detection in real-world environments via particle impact electrochemistry. *ACS Sens.* **2019**, *4*, 464–470. [CrossRef] [PubMed]
32. Cepriá, G.; Pardo, J.; Lopez, A.; Peña, E.; Castillo, J.R. Selectivity of silver nanoparticle sensors: Discrimination between silver nanoparticles and Ag+. *Sens. Actuators B Chem.* **2016**, *230*, 25–30. [CrossRef]
33. Stuart, E.J.E.; Kristina, T.; Joanna, E.; Compton, R.G. Improving the Rate of Silver Nanoparticle Adhesion to 'Sticky Electrodes': Stick and Strip Experiments at a DMSA-Modified Gold Electrode. *Electroanalysis* **2014**, *26*, 285–291. [CrossRef]
34. Stuart, E.J.E.; Zhou, Y.G.; Rees, N.V.; Compton, R.G. Determining unknown concentrations of nanoparticles: The particle-impact electrochemistry of nickel and silver. *RSC Adv.* **2012**, *2*, 6879–6884. [CrossRef]

Disclaimer/Publisher's Note: The statements, opinions and data contained in all publications are solely those of the individual author(s) and contributor(s) and not of MDPI and/or the editor(s). MDPI and/or the editor(s) disclaim responsibility for any injury to people or property resulting from any ideas, methods, instructions or products referred to in the content.